



Unveiling the Population of Wandering Black Holes via Electromagnetic Signatures

Angelo Ricarte^{1,2} , Michael Tremmel³ , Priyamvada Natarajan^{3,4,2} , and Thomas Quinn⁵

¹ Center for Astrophysics|Harvard & Smithsonian, 60 Garden Street, Cambridge, MA 02138, USA; angelo.ricarte@cfa.harvard.edu

² Black Hole Initiative, 20 Garden Street, Cambridge, MA 02138, USA

³ Department of Astronomy, Yale University, 52 Hillhouse Avenue, New Haven, CT 06511, USA

⁴ Department of Physics, Yale University, P.O. Box 208121, New Haven, CT 06520, USA

⁵ Department of Astronomy, University of Washington, P.O. Box 351580, Seattle, WA 98195, USA

Received 2021 April 26; revised 2021 June 23; accepted 2021 June 25; published 2021 August 2

Abstract

While most galaxies appear to host a central supermassive black hole (SMBH), they are expected to also contain a substantial population of off-center “wandering” SMBHs naturally produced by the hierarchical merger-driven process of galaxy assembly. This population has been recently characterized in an analysis of the ROMULUS cosmological simulations, which correct for the dynamical forces on SMBHs without artificially pinning them to halo centers. Here we predict an array of electromagnetic signatures for these wanderers. The predicted wandering population of SMBHs from ROMULUS broadly reproduces the observed spatial offsets of a recent sample of hyperluminous X-ray sources. We predict that the sources with the most extreme offsets are likely to arise from SMBHs within satellite galaxies. These simulations also predict a significant population of secondary active galactic nuclei (AGNs) with luminosities at least 10% that of the central AGN. The majority of galaxies at $z=4$ that host a central AGN with bolometric luminosity $L_{\text{bol}} > 10^{42} \text{ erg s}^{-1}$ are predicted to host a companion off-center AGN of comparable brightness. We demonstrate that stacked X-ray observations of similar mass galaxies may reveal a halo of collective emission attributable to these wanderers. Finally, because wanderers dominate the population of SMBHs with masses of $\lesssim 10^7 M_{\odot}$ in ROMULUS, they may dominate tidal disruption event (TDE) rates at these masses if they retain a stellar component (e.g., a nuclear star cluster). This could warrant an order of magnitude correction to current theoretically estimated TDE rates at low SMBH masses.

Unified Astronomy Thesaurus concepts: Supermassive black holes (1663); Active galactic nuclei (16); AGN host galaxies (2017); Hydrodynamical simulations (767)

1. Introduction

Massive galaxies are believed to host central supermassive black holes (SMBHs), which are important for regulating gas cooling via active galactic nucleus (AGN) feedback (e.g., Kormendy & Ho 2013). When one galaxy merges with another, its central SMBH begins a journey across many orders of magnitude in spatial scale that can eventually lead to a SMBH merger (Begelman et al. 1980). First, dynamical friction grinds down SMBH orbits on kiloparsec scales (Chandrasekhar 1943). When dynamical friction becomes less efficient on sub-kiloparsec scales, a variety of phenomena such as spherical asymmetry or the presence of gas are proposed to bridge the “final parsec problem” (e.g., Armitage & Natarajan 2002; Holley-Bockelmann & Khan 2015). Finally, gravitational wave emission takes over to shrink the binary orbit and drive sufficiently tight binaries together until they merge. To make robust predictions for gravitational wave events detectable by pulsar timing arrays (Hobbs et al. 2010; Arzoumanian et al. 2020) or the upcoming Laser Interferometer Space Antenna (LISA; Amaro-Seoane et al. 2017) mission, it is essential to understand all steps of this complex process.

Cosmological simulations, wherein SMBHs and galaxies self-consistently evolve in near realistic environments, are excellent tools for addressing the first part of this journey. Many numerical studies have revealed that significant delays can occur at the dynamical friction step (e.g., Holley-Bockelmann et al. 2010; Volonteri et al. 2016; Tamfal et al. 2018; Tremmel et al. 2018b; Bellovary et al. 2021). This is especially true in clumpy, high-redshift galaxies, which may make it difficult for offset SMBHs to reach galactic centers (Biernacki et al. 2017; Tremmel et al. 2018b; Pfister et al. 2019; Bortolas et al. 2020; Ma et al. 2021).

We term any SMBH that is spatially offset from its galactic center a “wandering” SMBH.

The ROMULUS cosmological simulations are ideally suited for studying this particular problem due to its careful treatment of SMBH dynamics, which correct for dynamical friction errors that naturally arise due to gravitational softening and limited mass resolution (Tremmel et al. 2015). This is in contrast with most cosmological simulations, which artificially and unphysically force SMBHs to be at the centers of their host galaxies. Some exceptions include MAGNETICUM (Hirschmann et al. 2014; Steinborn et al. 2016), HORIZON-AGN (Dubois et al. 2014; Bartlett et al. 2021), and recent simulations by Chen et al. (2021). The larger gravitational softening length of MAGNETICUM results in SMBHs artificially displaced by several kpc. Meanwhile, HORIZON-AGN includes dynamical friction from gas, but not dark matter and stars, whereas the reverse is true for ROMULUS.

Previous work with the ROMULUS simulations has shown that SMBHs can spend Gyrs offset from the galactic center following a galaxy merger (Tremmel et al. 2018b). Many SMBHs never make it to the centers of their galaxies, leading to a suppressed SMBH merger rate (Barausse et al. 2020). This results in a population of wandering SMBHs, as studied in Milky Way-like galaxies at $z=0$ in Tremmel et al. (2018a). ROMULUS successfully reproduces observed stellar mass-halo mass and SMBH mass-stellar mass relations from dwarf to galaxy-cluster scales. The simulations also produce cosmological star formation and SMBH growth histories that are consistent with observations, as well as realistic properties for the circumgalactic and intracluster media (Tremmel et al. 2017, 2019; Butsky et al. 2019; Ricarte et al. 2019; Sanchez et al. 2019;

Chadayammuri et al. 2021). These simulations are among the highest resolution of their class, resolving dwarf galaxies as small as $10^7 M_\odot$ in stellar mass with hundreds of star particles and tens of thousands of dark-matter particles. This high resolution allows SMBHs to be seeded within low-mass galaxies at $z > 5$ based solely on local gas properties and with no a priori assumptions about halo occupation (Tremmel et al. 2017). This results in a black hole occupation fraction that is purely a prediction of the simulation, and which correctly matches the current best estimates from observations (Ricarte et al. 2021). Thanks to this albeit simple seeding prescription, SMBH evolution can be tracked within low-mass, high-redshift galaxies, which are important contributors to overall SMBH merger rates (Volonteri et al. 2020), as well as long-lived, wandering SMBHs (Tremmel et al. 2018a, 2018b). To our knowledge, there is no other published cosmological simulation that seeds SMBHs based on local gas properties in a way that matches the observationally estimated SMBH occupation fraction and also allows SMBHs to wander their hosts with the addition of a dynamical friction correction.

We recently studied the broad demographics of the wandering population in ROMULUS, and found they exist in numbers proportional to the host halo mass, were distributed widely throughout the halo, and tended to stay near their initial seed mass in the simulation (Ricarte et al. 2021). In this work, we present observational predictions for detecting this population. Although previous work with these simulations concluded that detecting wanderers using razor-thin lensing arcs is infeasible (Banik et al. 2019), we find that wanderers in ROMULUS can manifest as hyperluminous X-ray sources (HLXs; e.g., King & Dehnen 2005; Barrows et al. 2019), spatially offset AGN (e.g., Comerford et al. 2009; Koss et al. 2012; Mezcua & Domínguez Sánchez 2020; Reines et al. 2020), and a faint halo of potentially detectable emission around a typical galaxy. If wanderers retain their stellar counterparts, they may also produce off-center tidal disruption events (TDEs).

2. Methods

Here, we briefly summarize the most important aspects of the SMBH physics in the ROMULUS simulations. Additional details can be found in Tremmel et al. (2017, 2019), where these simulations are introduced and described in detail. The ROMULUS simulations consist of ROMULUS25, a $(25 \text{ Mpc})^3$ volume, and ROMULUSC, a zoom-in simulation of a $10^{14} M_\odot$ galaxy cluster, both run under a cosmology with $\Omega_0 = 0.3086$, $\Lambda = 0.6914$, $h = 0.6777$, $\sigma_8 = 0.8288$. Both simulations have a mass resolution of $3.39 \times 10^5 M_\odot$ and $2.12 \times 10^5 M_\odot$ for dark matter and gas, respectively, and employ a spline gravitational softening length of 350 pc (equivalent to ~ 250 pc plummer softening). Unlike most other currently available simulations of this scale, SMBHs are seeded based on local gas properties, are not explicitly tethered to the centers of their host galaxies, and grow in a way that accounts for the resolved nearby gas kinematics.

2.1. SMBH Dynamics and Mergers

Central to this work is the fact that SMBH dynamical evolution can be accurately tracked down to sub-kpc scales in this simulation suite. This is done via a sub-grid correction that accounts for unresolved dynamical friction from stars and dark matter (Tremmel et al. 2015). This frictional force is estimated

by assuming a locally isotropic velocity distribution and integrating Chandrasekhar's equation (Chandrasekhar 1943) from the 90° deflection radius, r_{90} , out to the gravitational softening length, ϵ_g ,⁶ of the SMBH. This results in an acceleration applied to each SMBH particle in the simulation given by

$$\mathbf{a}_{\text{DF}} = -4\pi G^2 \rho (v < v_{\text{BH}}) \ln \Lambda \frac{\mathbf{v}_{\text{BH}}}{v_{\text{BH}}^2}, \quad (1)$$

where $\ln \Lambda = \ln(\frac{\epsilon_g}{r_{90}})$, v_{BH} is the SMBH's velocity relative to the local center of mass velocity of the closest 64 star and dark-matter particles, ρ is the mass density, and G is the gravitational constant. This correction, combined with the high dark-matter and stellar mass resolution in the simulations, results in realistic sinking timescales for off-center SMBHs (Tremmel et al. 2015, 2018b).

We adopt the SMBH merger criteria derived by Bellovary et al. (2010), in which two SMBHs merge if they approach within 0.7 kpc of one another (or, twice the gravitational softening length of 350 pc) and are also mutually bound ($\frac{1}{2} \Delta \mathbf{v} < \Delta \mathbf{a} \cdot \Delta \mathbf{r}$). The limit of 0.7 kpc is justified because at separations smaller than this distance we no longer trust the simulation to correctly model the dynamics of the system, as the gravitational force between the black holes becomes increasingly unresolved. When a merger occurs, the masses of the two SMBHs are added together and the resulting SMBH is given a position and velocity such that momentum is conserved (neglecting potential recoil due to gravitational wave emission).

2.2. SMBH Seeding

SMBHs are seeded in gas that has reached high densities ($3 m_p \text{ cm}^{-3}$, 15 times the threshold for star formation in ROMULUS) while being free of metals and still at relatively high temperatures (9500–10,000 K). This method selects gas with high Jeans mass that is also collapsing quicker than the typical timescale on which such a dense gas particle will form a star ($\sim 10^6$ yr). This is meant to roughly approximate the formation processes suggested by massive initial seeding models including direct collapse (Lodato & Natarajan 2007; Alexander & Natarajan 2014; Natarajan 2021) and results in SMBHs that are seeded preferentially at $z > 5$ within low-mass galaxies (Tremmel et al. 2017). Ricarte et al. (2021) show that the resulting $z=0$ SMBH occupation fraction matches estimates based on current observations down to dwarf-galaxy scales.

The initial mass of a SMBH is set to $10^6 M_\odot$, with each SMBH consuming nearby gas particles to account for their mass. This mass is somewhat higher than what is typically assumed even for the most massive direct-collapse formation scenarios, but it is required that the mass be at least a few times larger than the background dark matter and star particles to avoid spurious scattering events (Tremmel et al. 2015). It is possible that such large masses affect the growth history of these SMBH, but Ricarte et al. (2019) showed that the SMBH growth depends mostly on the galaxy properties, rather than the SMBH mass. It may also affect their dynamical evolution, but Tremmel et al. (2018a) showed that even with their relatively large masses, the wandering SMBH population has dynamical

⁶ Within this region, gravity is artificially reduced in order to avoid unrealistic, collisional behavior.

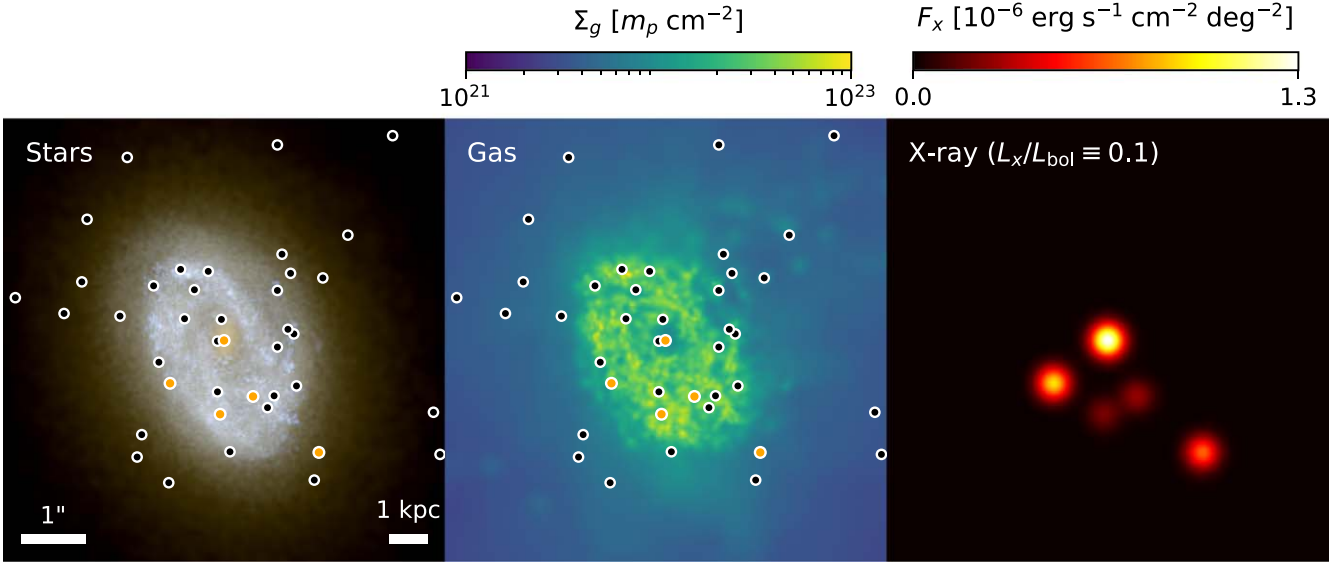


Figure 1. Example of a remarkable galaxy at $z = 0.1$ that hosts five SMBHs each shining with a bolometric luminosity above $10^{42} \text{ erg s}^{-1}$. Black and orange circles demarcate the projected positions of SMBHs bound to this galaxy’s halo, with orange circles marking those with $L_{\text{bol}} > 10^{42} \text{ erg s}^{-1}$. The brightest SMBH (at the center) shines at $L_{\text{bol}} = 3.7 \times 10^{43} \text{ erg s}^{-1}$. From left to right, we plot an image of stars with a surface brightness limit of $24 \text{ mag arcsec}^{-2}$, the integrated gas surface density, and a simulated X-ray image. In the X-ray image, we assume that 10% of the bolometric luminosity is emitted in some X-ray band, and that the observing instrument has a PSF with a FWHM of $0''.5$, appropriate for the center of the Chandra field of view. Despite the large number of accreting sources, there is no obvious morphological sign of a merger.

friction sinking timescales much longer than a Hubble time in $z = 0$, MW-mass halos.

2.3. SMBH Growth and Feedback

A SMBH’s accretion rate is estimated according to a Bondi–Hoyle–Lyttleton prescription (Bondi 1952), modified to account for angular momentum support. Specifically, the accretion rate is given by

$$\dot{M}_* = \alpha(n) \begin{cases} \frac{\pi(GM_*)^2 \rho}{(v_{\text{bulk}}^2 + c_s^2)^{3/2}} & \text{if } v_{\text{bulk}} > v_{\theta} \\ \frac{\pi(GM_*)^2 \rho c_s}{(v_{\theta}^2 + c_s^2)^2} & \text{if } v_{\text{bulk}} < v_{\theta}, \end{cases} \quad (2)$$

where G is the gravitational constant, M_* is the SMBH mass, ρ is the ambient mass density, c_s is the ambient sound speed, v_{θ} is the local rotational velocity of surrounding gas, and v_{bulk} is the bulk velocity relative to the SMBH. The coefficient $\alpha(n)$ provides a boost to the accretion rate given by

$$\alpha(n) = \begin{cases} \left(\frac{n}{n_{\text{th},*}}\right)^2 & \text{if } n \geq n_{\text{th},*} \\ 1 & \text{if } n < n_{\text{th},*} \end{cases} \quad (3)$$

where $n_{\text{th},*}$ is the star formation number density threshold, below which the simulation no longer resolves the multi-phase interstellar medium, as in Booth & Schaye (2009). During the accretion process, thermal energy is injected isotropically into the surrounding gas particles, assuming a radiative efficiency of 10% and a feedback coupling efficiency of 2%. We adopt the same radiative efficiency when computing bolometric luminosities, such that $L_{\text{bol}} = 0.1 \dot{M}_* c^2$.

2.4. Selection of Dark-matter Halos and Wandering SMBHs

We follow the post-processing performed in Ricarte et al. (2021), using the AMIGA halo finder to identify structures (Knollmann & Knebe 2009), PYNBODY for particle data analysis (Pontzen et al. 2013), and TANGOS for the construction of a database of galaxy and SMBH properties (Pontzen & Tremmel 2018). As in this previous study, we designate a SMBH as a “wanderer” if it is further than 0.7 kpc (twice the gravitational softening length) from the center of its host halo, which is identified using a shrinking spheres method (Power et al. 2003). This distance threshold is used because the center of the galaxy/halo becomes ill defined within 0.7 kpc at the gravitational force resolution of ROMULUS. Further, we want to avoid selecting wandering SMBHs that may be about to merge with another SMBH (see Section 2.1 above).

3. Results

In the ROMULUS simulations, SMBHs accrete according to the Bondi formula regardless of their positions in the halo. For many galaxies, this may result in a very faint halo of emission, further explored in Section 3.3. In Figure 1, we plot a more striking example of a galaxy hosting five SMBHs each with bolometric luminosities $L_{\text{bol}} > 10^{42} \text{ erg s}^{-1}$ when accretion rates are averaged over 30 Myr. For this luminosity threshold, this galaxy hosts the most AGN at this snapshot, $z = 0.1$. The brightest SMBHs are simply the most massive ones in the halo, each SMBH having grown to a mass of $10^7 M_{\odot}$ or higher, while the median wanderer mass is near the seed mass of $10^6 M_{\odot}$. In the right panel, we simulate an X-ray image by assuming that 10% of the bolometric luminosity is emitted in some X-ray band (e.g., Hopkins et al. 2007), and that the instrument has a point-spread function (PSF) with a FWHM of $0''.5$, appropriate for Chandra. As shown in Tremmel et al. (2018b), SMBHs can remain offset in the ROMULUS simulations Gyrs after the halo mergers that deposited them occurred. We emphasize that the wandering SMBHs considered in this

study are not necessarily associated with active galaxy mergers. Despite the large number of accreting SMBHs in Figure 1, the host galaxy morphology resembles an ordinary spiral with a stellar mass of $1.0 \times 10^{11} M_{\odot}$ and no obvious merger signatures.

3.1. Comparison to Hyperluminous X-Ray (HLX) Sources

Accreting, wandering black holes, like those shown in Figure 1, can manifest as HLXs. These are off-nuclear X-ray sources with X-ray luminosities above $10^{41} \text{ erg s}^{-1}$ (Kaaret et al. 2001; Matsumoto et al. 2001; Gao et al. 2003). As the most extreme tail of the ultraluminous X-ray (ULX) population, these sources are unlikely to be produced by stellar mass objects and may instead represent accreting wandering SMBHs (King & Dehnen 2005). Masses in the intermediate black hole mass range ($M_{\text{BH}} < 10^6 M_{\odot}$) are also supported by X-ray spectral fitting, which in turn imply relatively low blackbody temperatures (Miller et al. 2003; Davis et al. 2011).

Barrows et al. (2019) assembled a sample of 169 HLXs by cross-matching galaxies with known redshifts in the Sloan Digital Sky Survey (SDSS) with the Chandra Source Catalog (Evans et al. 2010). This sample includes sources with hard X-ray luminosities in excess of $10^{41} \text{ erg s}^{-1}$ in the 2–10 keV band up to $z \sim 0.9$. Barrows et al. (2019) conservatively keep only those X-ray sources that are offset by ≥ 5 times the uncertainty of their positions relative to their host galaxy centroids, which varies from source to source. Most HLXs in this sample exhibit offsets of tens of kpc.

In Figure 2, we compare the distribution of offsets obtained from this work with ROMULUS25. In black, we plot the distribution of offsets from Barrows et al. (2019), with each source weighted by the factor $(1 - f)$, where f is their estimated contamination fraction of each source. The red histogram is the distribution of offsets in the ROMULUS25 simulation obtained when emulating their selection criteria. For this comparison, we first select galaxies with rest frame $r < 22.5$ for all snapshots with redshifts $z < 0.9$, to mimic the pre-selection of galaxies in the SDSS. Then, we search for every SMBH within the virial radius of each selected halo, even if it is within a satellite halo. If its bolometric luminosity averaged over the past 30 Myr is at least $10^{42} \text{ erg s}^{-1}$, (that is, if its X-ray luminosity is at least $10^{41} \text{ erg s}^{-1}$ assuming a bolometric correction of 10%), we consider it detectable and save its offset from the center of the halo. The three-dimensional spatial distribution of HLXs is then projected onto the sky using an Abel transform, and each redshift snapshot n in the simulation between $0.05 < z < 0.9$ is volume-weighted by redshift.⁷ These distributions are normalized to integrate to unity.

Comparing the red ROMULUS25 predicted distribution to the observed HLX distribution shown in black, we do indeed reproduce a population of luminous wandering SMBHs with separations of tens of kpc, as observed in Barrows et al. (2019). The most extreme offset SMBHs typically reside in the outskirts of the halos of massive galaxies, with stellar masses $> 10^{11.4} M_{\odot}$. However, unlike the observations, we find that this distribution should continue to increase with decreasing projected separation. This implies the existence of a much larger population of

⁷ Each redshift slice is assigned a weight $dV/dn = (dV/dz)(dz/dn)$, where $dV/dz = cd_L^2(1+z)^{-1}dt/dz$ is the evolution of the comoving volume element with redshift, and dz/dn is the frequency with which redshifts are sampled in the simulation outputs. Here, c is the speed of light and d_L is the luminosity distance.

moderately offset sources missed observationally by current campaigns (Barrows et al. 2019). This is most likely a selection effect due to limited astrometric precision, as discussed further in Stemo et al. (2020).

Using the AMIGA halo finder, we can assess the fraction of detectable HLXs in the simulation that are “true” wanderers bereft of any resolved subhalo, as opposed to those that only appear as wanderers because they reside in nearby satellite galaxies too faint to have been detected. In the blue histogram of Figure 2, we repeat the analysis done to produce the red histogram, but omit any SMBHs that actually reside in a subhalo detected by our halo finder. This distribution declines more rapidly with radius, indicating that the most offset HLXs likely reside in faint satellite galaxies. We plot the fraction of wanderers lacking a subhalo in the simulation as a function of projected halo-centric distance in the top panel. We find that this fraction stays above 50% until a projected separation of 15 kpc.

For HLXs with subsequently identified optical counterparts, Barrows et al. (2019) also considered the SMBH mass (M_{\bullet}) to stellar mass (M_*) relation for their sources. Lacking a more direct measurement of M_{\bullet} , they estimated M_{\bullet} by assuming that the HLXs accrete with an Eddington ratio of 0.24, motivated by the average X-ray spectral index observed and a relationship between spectral index and Eddington ratio (Greene & Ho 2007). We perform the same selection on our ROMULUS25 HLXs, which have an identifiable subhalo (those that are part of the inventory in the red histogram, but not the blue one, in Figure 2). In Figure 3, we plot the SMBH mass to stellar mass relation for the subset of the Barrows et al. (2019) sample with identified stellar counterparts as solid blue circles, where error bars have been omitted for clarity. We plot the SMBH mass as a function of host stellar mass in the ROMULUS25 simulation in orange, computed in a different way in each of the panels. In the left panel, we plot each SMBH’s accreted mass⁸ in the simulation, which has been found to trace the $M_{\bullet} - M_*$ relation in ROMULUS even below the seed mass of $10^6 M_{\odot}$ and can be interpreted as a proxy for the true black hole mass in dwarf galaxies (Ricarte et al. 2019). (See Appendix A and Figure 7 for a comparison of accreted and raw SMBH masses among our wanderers.) Barrows et al. (2019) found that their sources were broadly consistent with AGN in low-mass galaxies, the relationship found by Reines & Volonteri (2015), shown as a green dashed line. Similarly, we find that the accreted masses of ROMULUS25 HLXs are also consistent with typical galaxies of the same mass. Here, the appropriate comparison is actually the relationship found by Schramm & Silverman (2013) shown in red, which is the relation used to calibrate the SMBH accretion and feedback parameters in ROMULUS. This reproduction is not entirely trivial, as environmental processes could have potentially modified this relationship for galaxies in these subhalos.

In the right panel, we emulate the Barrows et al. (2019) proxy by “estimating” masses from SMBH luminosities assuming an Eddington ratio of 0.24. We find that this would have caused us to greatly underestimate ROMULUS25 masses, because ROMULUS25 SMBHs tend to have much lower Eddington ratios than this adopted value (Ricarte et al. 2019).

⁸ A SMBH’s accreted mass is the portion of mass acquired purely from gas accretion, excluding any number of seed masses that have merged to form the final product.

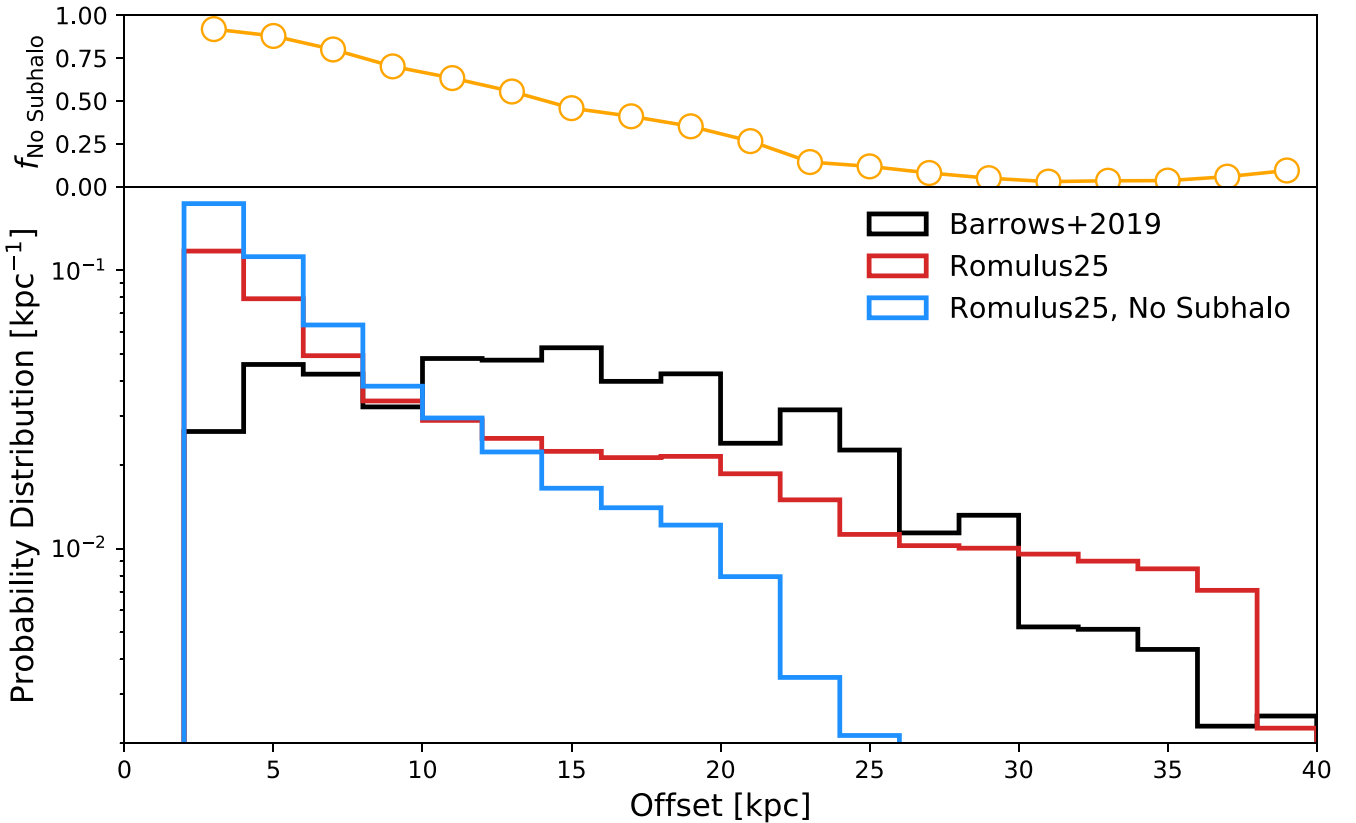


Figure 2. Comparison of ROMULUS25 predicted offset distributions to the detected HLX sample of Barrows et al. (2019), all normalized to integrate to unity. In black, we plot the distribution of observed sources from Barrows et al. (2019). In red, we plot the projected distribution of offsets from ROMULUS emulating their selection, considering galaxies with $r < 22.5$, $0.05 < z < 0.9$, and $L_{\text{bol}} > 10^{42} \text{ erg s}^{-1}$ when averaged over 30 Myr. We reproduce a broad distribution of offsets, but find that the true distribution should peak at small radii with sources likely missing due to limited astrometric precision. In blue, we plot the distribution for the subset of wanderers that are not considered to reside within a resolved subhalo (satellite galaxy) in the simulation, revealing that the most extreme offsets are most likely to arise from interloping faint galaxies. In the top panel, we plot the fraction of apparently offset SMBHs that lack an accompanying subhalo, and find that this function drops below 50% at separations of $\gtrsim 15$ kpc.

That is, ROMULUS HLXs tend to be fainter than those in Barrows et al. (2019) at a given SMBH mass.

The overall good agreement between Romulus predictions and the observed HLXs lends us confidence in the robustness of the simulated properties of the off-center SMBH population. In subsequent sections, we explore the key electromagnetic properties of the wandering population in Romulus.

3.2. Occurrence Rates of Dual AGN

Dual AGN are ubiquitous in the ROMULUS universe, at least at low luminosities where we can build meaningful statistics. In Figure 4, we plot the probability of there being a second AGN in a galaxy with a (bolometric) luminosity at least $L_2 > RL_1$, given that there is already a first AGN with a luminosity of at least $L_1 > 10^{42} \text{ erg s}^{-1}$. We plot the luminosity of these wanderers as a function of host stellar mass across several redshifts. Two brightness ratios are provided, $R = 1/2$ in orange and $R = 1/10$ in purple. Error bars are estimated via bootstrapping in each stellar mass bin. Although a bolometric luminosity threshold of $10^{42} \text{ erg s}^{-1}$ is quite low, we are unfortunately limited by the relatively small (25 Mpc)³ volume of ROMULUS25, which also does not produce many high Eddington ratio systems (Ricarte et al. 2019).

In ROMULUS25, a galaxy hosting an SMBH with $L_{\text{bol}} > 10^{42} \text{ erg s}^{-1}$ at $z = 0.05$ has a roughly 10% chance of hosting a second SMBH shining with at least one-tenth the first's luminosity. However, we predict that dual AGN should be

much more common at higher redshifts, motivating deep surveys and sensitive instruments capable of testing this prediction. At present, searches for spatially resolved dual AGN in the X-ray are confined to $z \lesssim 0.05$ and $R \gtrsim 0.01$ (Foord et al. 2019, 2021). Yet at $z = 4$, the *majority* of galaxies in ROMULUS with one SMBH above this luminosity threshold host another with at least 10% of its luminosity. We have tested increasing the luminosity threshold to $L_1 = 10^{43} \text{ erg s}^{-1}$, and did not find any noticeable difference aside from poorer statistics. SMBH accretion rates are averaged over 30 Myr in Figure 4, but it is possible for AGN to have shorter duty cycles than this. To interpret these results assuming that the AGN only shine a fraction D of the time, L_1 should be multiplied by a factor $1/D$ to conserve the average accretion rate, but the dual AGN probability must be correspondingly divided by the same factor.

3.3. Average Wanderer Emission Profiles

If wandering SMBHs prove to be difficult to find and resolve individually, they may likely manifest as a “halo” of emission or excess counts in stacked images. In Figure 5, we compute the average emission profile of wandering SMBHs that one would obtain by stacking halos of similar mass. Once again, we average wandering SMBH accretion rates over a 30 Myr timescale, and further assume that 10% of the radiated energy is emitted in the 2–10 keV X-ray band (e.g., Hopkins et al. 2007). We perform an Abel transform to project average spherical

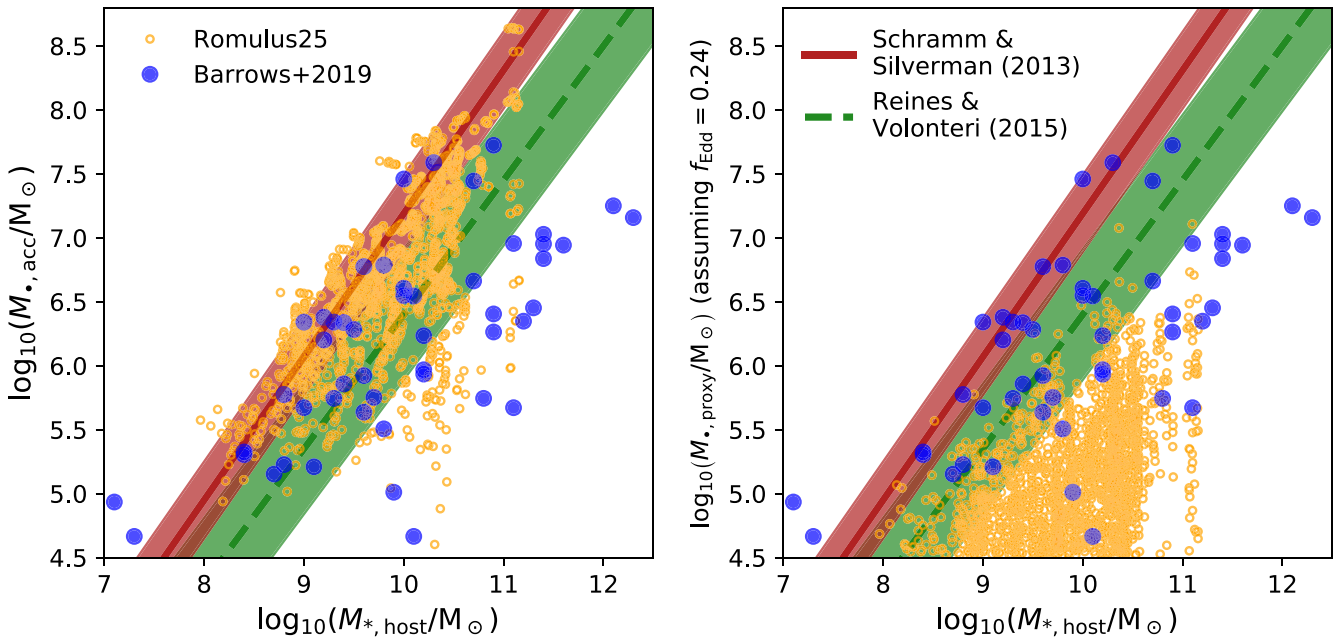


Figure 3. Comparison of the $M_* - M_*$ relation for HLXs in the Barrows et al. (2019) sample (blue) compared to ROMULUS25 (orange). The Barrows et al. (2019) sample plotted here only includes those HLXs with optically identifiable stellar counterparts in their study. They found their sources to be broadly consistent with the relationship observed by Reines & Volonteri (2015), shown as a dashed green line. In the left panel, we find that accreted masses of ROMULUS25 HLXs are also broadly consistent with typical galaxies, but they are calibrated to a different relationship, shown as the red solid line (Schramm & Silverman 2013). In Barrows et al. (2019), SMBH masses are estimated by assuming that they accrete with a uniform Eddington ratio of 0.24, motivated by their X-ray spectral indices. In the right panel, we perform a more direct comparison with the ROMULUS simulations by also applying this proxy and “estimating” SMBH masses based on their accretion rates, averaged over 30 Myr. We find that this would have caused us to greatly underestimate ROMULUS25 SMBH masses, since ROMULUS wanderers typically accrete at much lower Eddington ratio and are therefore fainter than these HLXs (Ricarte et al. 2019).

profiles onto the plane of the sky, and apply the appropriate cosmological factors due to the evolving luminosity and angular diameter distances with redshift to derive this estimate. Each color represents a different bin in halo mass, as indicated by the legend.

At $z = 0.05$, halos in the $10^{11-13} M_\odot$ mass range exhibit average wandering light profiles orders of magnitude above the cosmic X-ray background, plotted in gray. The solid horizontal line represents the cosmic X-ray background levels in the 2.0–10.0 keV band (Cappelluti et al. 2017). Dwarf galaxy halos (purple) have too few wanderers with too little luminosity, while the galaxy-cluster halo in ROMULUSC (orange) exhibits suppressed emission, as most galaxies are quenched and quiescent in the cluster environment (Tremmel et al. 2019). Unfortunately, although the ROMULUSC cluster hosts 1613 wandering SMBHs, they accrete less efficiently in its hotter halo (see also Ricarte et al. 2021, for further discussion of this phenomenon).

As thin dotted curves, we plot the average flux from central SMBHs, blurred assuming a Gaussian PSF with a FWHM of $0''.5$, appropriate for the center of the Chandra field of view. Additionally, as thin dashed curves, we plot the expected contribution from X-ray binaries (XRBs), for which details are provided in Section 3.1. At low enough redshift, these faint, extended halos of wanderer emission are much larger than the Chandra PSF and may extend to $\sim 10''$ above both the X-ray background and host galaxies’ XRBs. However, wanderers become too faint to detect above X-ray background levels by $z = 1$. This signal could potentially be detected by stacking X-ray observations centered on similar mass galaxies, masking out satellites, and comparing the resulting profiles to expectations from the field.

3.4. Wandering TDEs?

A TDE flare is caused by the destruction and accretion of a star torn apart by tidal forces when it approaches too close to a SMBH (Rees 1988). Several tens of TDEs have been observationally identified, and soon orders of magnitude more are expected from ongoing and future surveys such as the Zwicky Transient Factory and Vera Rubin Observatory (Strubbe & Quataert 2009; van Velzen et al. 2011; Bricman & Gomboc 2020). The number density of SMBHs as a function of mass is the basic ingredient needed to compute theoretical estimates of the volumetric TDE rate, and this has typically been derived from scaling relations between *central* SMBH masses and host galaxy properties (Stone & Metzger 2016; Stone et al. 2020). In this section, we demonstrate that the majority of SMBHs with masses $\lesssim 10^7 M_\odot$ are in fact wanderers, missed entirely by this kind of accounting. If these wandering SMBHs can retain stellar counterparts (such as their nuclear star clusters (NSCs)) and disrupt stars at comparable rates, then the majority of TDEs originating from SMBHs with $M_* < 10^7 M_\odot$ may be centrally offset.

In Figure 6, we plot the fraction of SMBHs of a given mass in ROMULUS25 that are centrals, for three different redshifts. We find that this fraction drops rapidly at low masses, such that at $z = 0.05$, only one in twelve $10^6 M_\odot$ SMBHs are centrally located. The central fraction decreases with decreasing redshift, as more minor mergers build up the wandering population. If (i) these statistics are representative of the real universe, (ii) wandering SMBHs disrupt stars at a comparable rate to centrals, and (iii) offset TDEs are equally identifiable, then the majority of TDEs due to SMBHs with $M_* < 10^7 M_\odot$ should be offset from their galactic centers.

This may require a significant upward revision of the theoretically estimated TDE rates, which we estimate here.

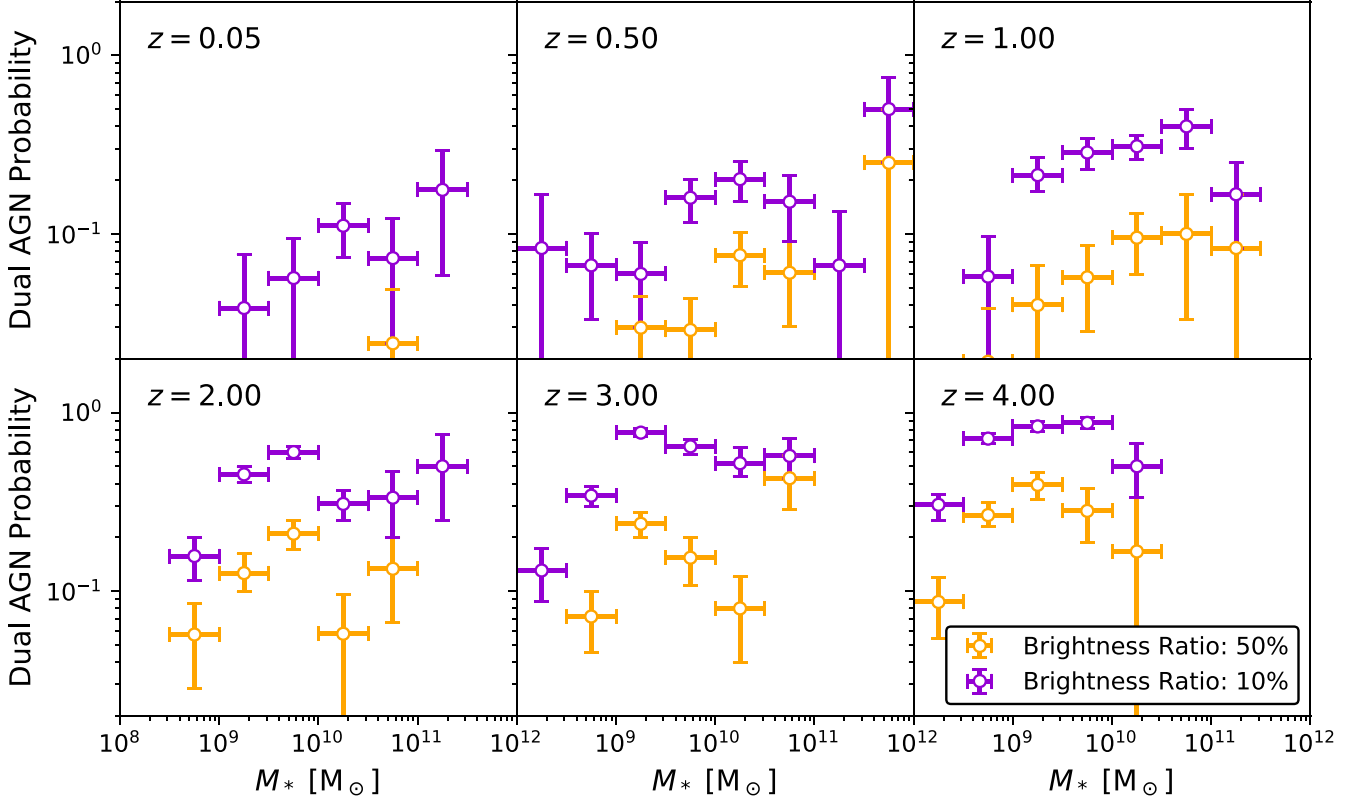


Figure 4. Given an AGN shining with a bolometric luminosity of $L_1 > 10^{42} \text{ erg s}^{-1}$, we plot the probability of there existing a second AGN in the same halo shining with a luminosity $L_2 > RL_1$ as a function of stellar mass and redshift. Two values of this luminosity ratio R are considered, 50% in orange and 10% in purple. We find that this probability increases with both stellar mass and redshift. Error bars originate from bootstrapping. At $z = 4$, most galaxies that host one SMBH above this threshold host another with at least 10% of the first's luminosity, motivating deep surveys and sensitive instruments capable of testing this prediction.

Stone & Metzger (2016) expressed the theoretical TDE rate as a function of SMBH mass as $N(M_*/10^8 M_\odot)^B$, where $N = 2.9 \times 10^{-5} \text{ yr}^{-1}$ and $B = -0.404$. Consequently, we can estimate this correction factor via $C = \sum_{\text{all}} M_*^B / \sum_{\text{cen}} M_*^B$, representing a sum over all SMBHs in ROMULUS25 in the numerator and a sum restricted to central SMBHs in the denominator. We find that the volumetric TDE rate when accounting for wandering SMBHs should be revised upward by a factor of $C = 8.0$ at $z = 0.05$, owing mostly to $10^6 M_\odot$ SMBHs, to which current surveys are not sensitive. This may even be an underestimate, because the black hole occupation fraction in dwarf galaxies is highly uncertain and may well be unity (e.g., Mezcua et al. 2018; Baldassare et al. 2020). On the other hand, this potential enhancement is larger than predicted by previous studies of ultra-compact dwarf galaxies, potentially due to differences in the SMBH occupation fraction (Voggel et al. 2019). At present, there exists one compelling offset TDE candidate, which is located 12.5 kpc from the center of a lenticular galaxy and exhibits a $L \propto t^{-5/3}$ light curve characteristic of TDEs (Lin et al. 2018). The occurrence rate of offset TDEs can place joint constraints on SMBH dynamics, the SMBH occupation fraction, and the NSC occupation fraction.

4. Discussion

We present observational comparisons and predictions for wandering SMBHs using the ROMULUS suite of cosmological simulations. These simulations carefully apply a corrective dynamical friction force onto SMBHs to produce realistic dynamics and implement a physically motivated seeding

prescription that produces SMBH occupation fractions consistent with observations. Our key findings are summarized as follows.

1. We compare the wandering population of ROMULUS25 to the Barrows et al. (2019) sample of HLXs. We reproduce a broad offset distribution, and find that most objects offset by more than 15 kpc are likely to be in satellite galaxies. The population of greatly offset HLXs in this sample also implies a much larger population with more modest offsets, which are more likely to lack a corresponding subhalo.
2. Dual AGNs are common in the ROMULUS universe at the low luminosities that these simulations can probe. The majority of galaxies at $z = 4$ containing an AGN shining above $L_{\text{bol}} > 10^{42} \text{ erg s}^{-1}$ also contain a second AGN of comparable brightness.
3. Wandering SMBHs may collectively manifest as an overdensity of X-ray emission around galaxies in excess of the cosmic background. Stacked X-ray observations of galaxies may reveal a faint halo of emission attributable to these wanderers.
4. Below $10^7 M_\odot$, central SMBHs of a given mass are greatly outnumbered by wanderers. If these wandering SMBHs can retain their nuclear star clusters, wanderers may dominate the TDE rate by low-mass SMBHs.

An important caveat for this work is the underlying assumption of Bondi-like accretion, a sub-grid prescription used in most cosmological simulations. Higher-resolution

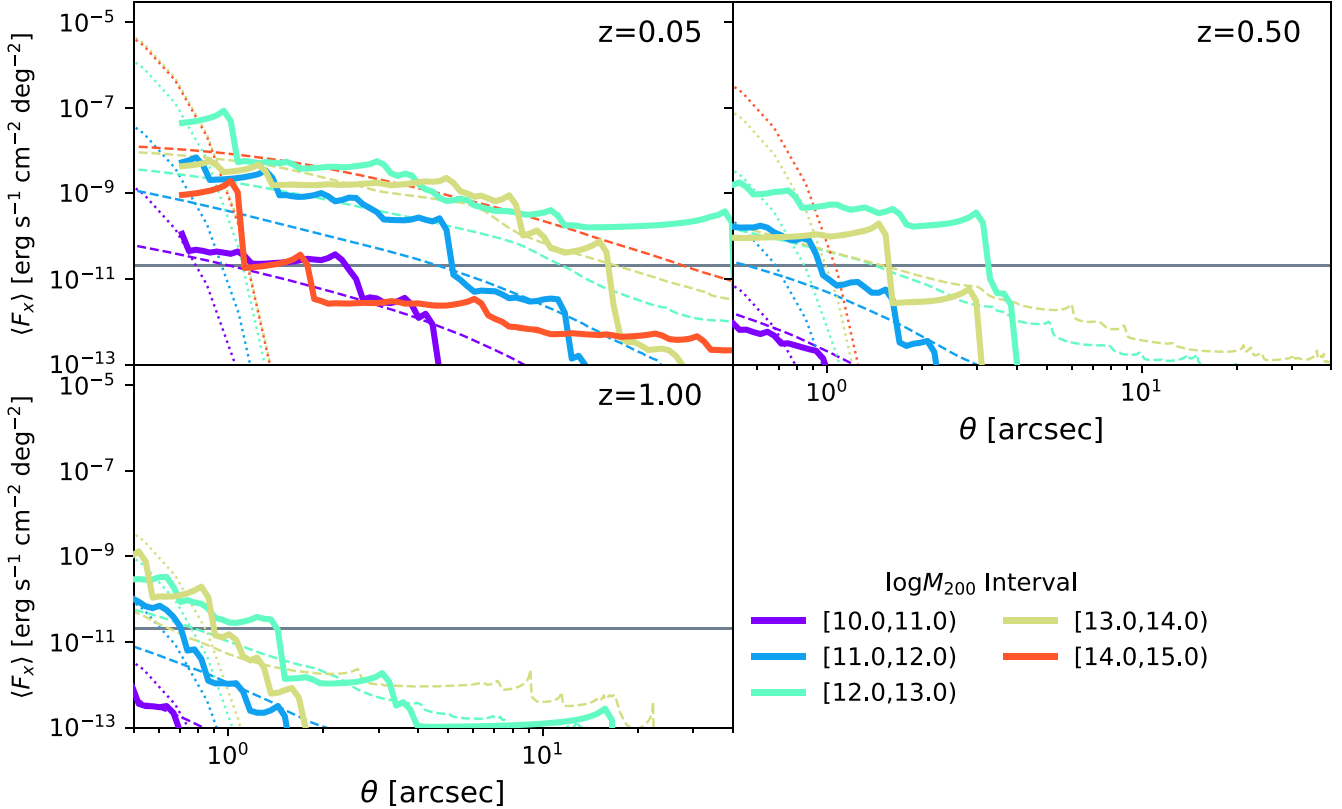


Figure 5. Predicted X-ray emission profiles due to accreting wandering SMBHs for different halo masses and redshifts. Solid colored lines plot 2–10 keV emission profiles from wandering SMBHs calculated by assuming a bolometric correction of 0.1 and averaging halos of similar mass. With thin dotted lines, we plot the average flux of central SMBHs among the same halos, convolved with a two-dimensional Gaussian PSF with a FWHM of 0''.5, appropriate for Chandra. Shown as thin dashed lines, we also estimate the contribution from XRBs based on empirical relations. Colors correspond to the halo masses averaged in each curve, as indicated in the legend. A gray horizontal line marks the cosmic X-ray background level in this X-ray band (Cappelluti et al. 2017). At small redshifts, ROMULUS predicts a profile of X-ray emission due to wandering SMBHs that is most strongly above both XRBs and the X-ray background in the halo mass range between $10^{11-13} M_{\odot}$.

simulations have demonstrated that the accretion rate onto wanderers may be limited to $\sim 10\%-20\%$ the Bondi rate due to the wide distribution of angular momentum encountered moving through the halo (Guo et al. 2020). Furthermore, if SMBH accretion rates are low enough for their disks to be in the advection-dominated regime, then the accumulation of magnetic flux around their horizons may further suppress accretion rates by orders of magnitude (Igumenshchev & Narayan 2002; Perna et al. 2003; Pellegrini 2005; Ressler et al. 2021). The accretion and feedback prescriptions in these simulations successfully reproduce the empirical $M_{\bullet} - M_{*}$ scaling relation (Schramm & Silverman 2013), and we have previously shown that the typical luminous wanderer may have an Eddington ratio large enough to avoid forming an advection domination accretion flow (Ricarte et al. 2021). Nevertheless, as numerical techniques improve, it will be useful to compare the results from ROMULUS to other cosmological simulations with different sub-grid physics.

These simulations predict that dual AGN may be common at low luminosities and high redshifts, motivating deep studies that can test this prediction. Additional detailed comparisons of offset/dual AGN samples that carefully forward-model selection effects would be useful to calibrate theoretical uncertainties, such as the temporally unresolved AGN duty cycle. In our current work, we have not considered the velocities of wandering SMBHs. In galactic nuclei, velocities of the

measured double-peaked emission lines have been used to spectrally identify dual/offset AGN (e.g., Blecha et al. 2013; Comerford & Greene 2014; Pesce et al. 2021).

Ricarte et al. (2021) found that most wandering SMBHs in ROMULUS do not reside in *resolved* stellar overdensities, except for those at large radii which experience weaker tidal forces. However, our simulations cannot resolve the formation and disruption of structures below the gravitational softening length of 350 pc. Below these scales, SMBHs are expected to be accompanied by NSCs, especially in the mass ranges spanned by wandering SMBHs (Neumayer et al. 2020). van den Bosch & Ogiya (2018) argued that it is extremely difficult to completely disrupt the central regions of a halo in the cold dark-matter paradigm.

Due to limited resolution, our simulations lack two important channels to create wanderers, namely multi-body SMBH interactions (e.g., Volonteri et al. 2003) and gravitational wave recoil following SMBH mergers (e.g., Libeskind et al. 2006; Volonteri 2007; Holley-Bockelmann et al. 2008). These types of wanderers may dominate the wandering population at low halo-centric radius (Volonteri & Perna 2005; Izquierdo-Villalba et al. 2020).

In conclusion, simulations predict the existence of an extensive wandering SMBH population that stands to be revealed via their electromagnetic signatures. This work suggests that our current census of detected SMBHs is highly incomplete.

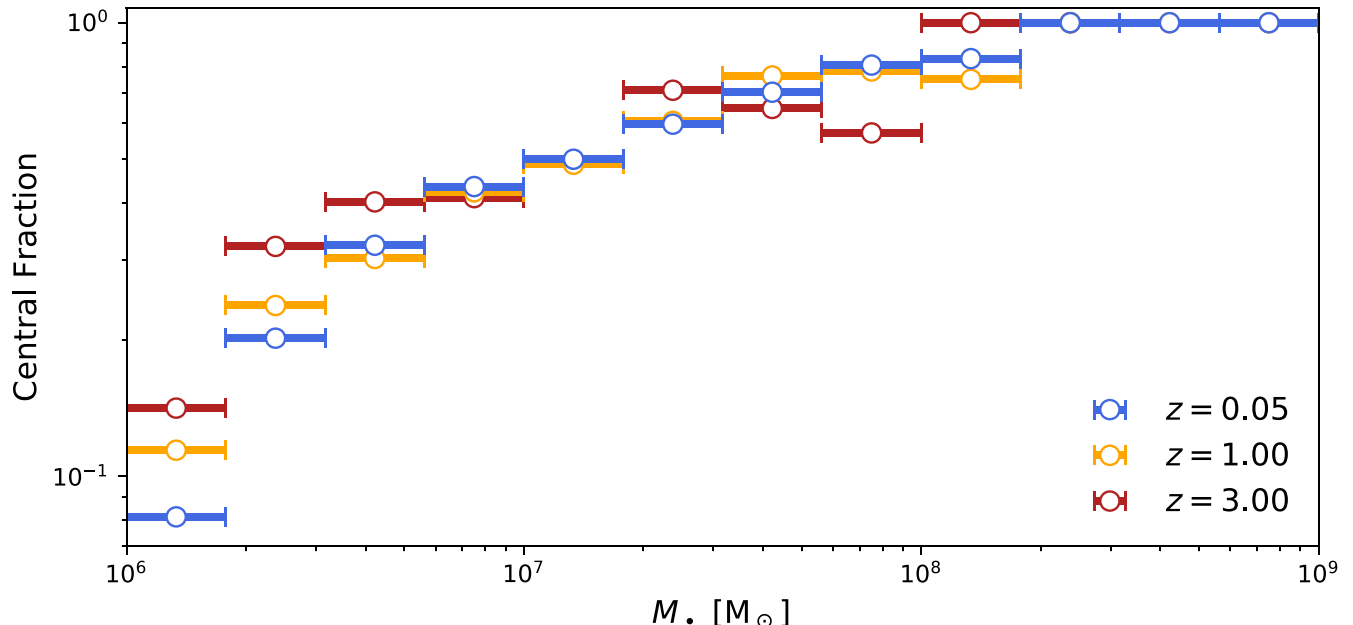


Figure 6. The fraction of SMBHs of a given mass that are centrally located in ROMULUS25. This fraction drops far below unity at low masses, meaning that the typical $10^6 M_\odot$ SMBH is actually a wanderer. If these wandering SMBHs are able to retain an unresolved stellar component, they may dominate the TDE rate in their mass bin.

We thank our anonymous referee for insightful comments that improved the presentation of our results. A.R. thanks Ramesh Narayan for continued support and insightful conversations about wandering SMBH accretion rates. We thank Nicholas Stone for fruitful conversations about TDEs, and Kristen Garofali for helpful conversations about X-ray emission of hot gas.

A.R. is supported by the National Science Foundation under grant No. OISE 1743747 as well as the black hole Initiative (BHI) by grants from the Gordon and Betty Moore Foundation and the John Templeton Foundation. M.T. is supported by an NSF Astronomy and Astrophysics Postdoctoral Fellowship under award AST-2001810. P.N. acknowledges hospitality and support from the Aspen Center for Physics, where some of the early ideas that informed this work were developed during the summer workshop titled “Emergence, Evolution and Effects of Black Holes in the Universe: The Next 50 Years of black hole Physics” that she co-organized. The Aspen Center for Physics is supported by National Science Foundation grant PHY-1066293. The ROMULUS simulations are part of the Blue Waters sustained-petascale computing project, which is supported by the National Science Foundation (awards OCI-0725070 and ACI-1238993) and the state of Illinois. Blue Waters is a joint effort of the University of Illinois at Urbana-Champaign and its National Center for Supercomputing Applications. This work is also part of a Petascale Computing Resource Allocations allocation support by the National Science Foundation (award number OAC-1613674). This work also used the Extreme Science and Engineering Discovery

Environment (XSEDE), which is supported by National Science Foundation grant number ACI-1548562. Resources supporting this work were also provided by the NASA High-End Computing (HEC) Program through the NASA Advanced Supercomputing (NAS) Division at Ames Research Center. Analysis was conducted on the NASA Pleiades computer and facilities supported by the Yale Center for Research Computing.

Data Availability

The data presented in this article will be available upon request.

Appendix A Raw versus Accreted Black Hole Masses in ROMULUS

In Figure 3, we compared the $M_\bullet - M_*$ relation observed for HLXs with subsequently detected host galaxies with that from the ROMULUS simulations. For this comparison, we used only the accreted portion of a SMBH’s mass, excluding seed masses. This is because the accreted mass in the ROMULUS simulations actually follows the $M_\bullet - M_*$ at low masses better than the raw mass, even below the seed mass of $10^6 M_\odot$ (Ricarte et al. 2019). In Figure 7, we compare the accreted mass $M_{\bullet, \text{acc}}$ with $M_{\bullet, \text{sim}}$, the raw SMBH from the ROMULUS simulations. While lower masses are pushed to values above the seed mass, we find general agreement.

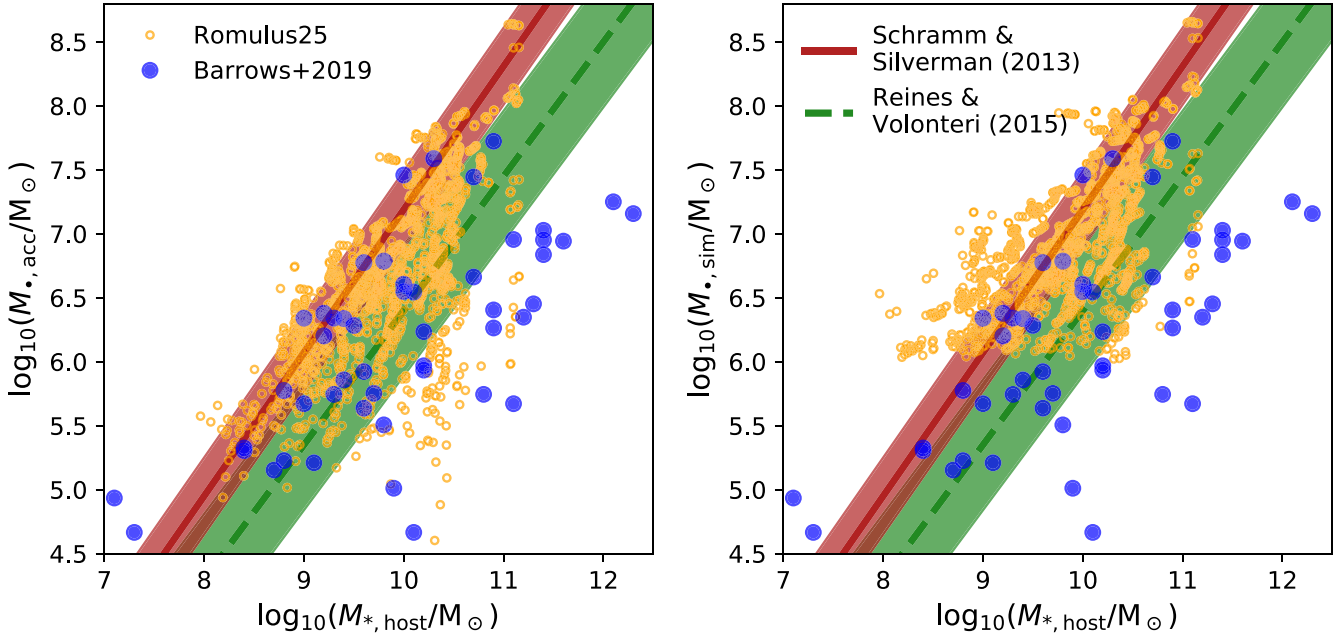


Figure 7. Here, we compare accreted (left panel) and raw (right panel) SMBH masses in the ROMULUS simulations in the context of Figure 3. As pointed out in Ricarte et al. (2019), the accreted mass follows the $M_{\bullet} - M_{\bullet}$ relation to which this simulation is calibrated even below the seed mass of $10^6 M_{\odot}$, making it a valuable proxy for the true SMBH mass in low-mass galaxies. If raw masses are used instead, as in the right panel, SMBH masses are all pushed above the seed mass, but we retain general agreement with the Schramm & Silverman (2013) relationship.

Appendix B Projected Flux Density Profiles

Here, we detail how we estimate the X-ray contribution to projected flux density profiles by XRBs. By analyzing the 6 Ms Chandra Deep Field South, Lehmer et al. (2016) arrive at the following relationship between the 2 and 10 keV X-ray luminosity L_x , galaxy stellar mass M_{\bullet} , star formation rate \dot{M}_{\bullet} , and redshift z :

$$\left(\frac{L_x}{\text{erg s}^{-1}} \right) = \alpha_0 (1 + z)^{\gamma} \left(\frac{M_{\bullet}}{M_{\odot}} \right) + \beta_0 (1 + z)^{\delta} \left(\frac{\dot{M}_{\bullet}}{M_{\odot} \text{ yr}^{-1}} \right). \quad (\text{B1})$$

where $\log \alpha_0 = 29.37 \pm 0.15$, $\log \beta_0 = 39.28 \pm 0.05$, $\gamma = 2.03 \pm 0.60$, and $\delta = 1.31 \pm 0.13$. In the ROMULUS simulations, we compute radial profiles of the stellar mass and star formation rate density and average these together for halos in a given halo mass bin. We apply Equation (B1) to transform these into X-ray luminosity density profiles in units of $\text{erg s}^{-1} \text{ cm}^{-3}$. An Abel transform is then required to turn this into a projected luminosity density profile $l_x(r)$ in units of $\text{erg s}^{-1} \text{ cm}^{-2}$.

The projected flux density profile is then obtained via $f_x = l_x / (4\pi d_L^2)$, where d_L is the luminosity distance. Finally, we transform between physical scales (r) and angular scales (θ) by computing the angular diameter distance, such that $\theta = r/d_A$. The final projected flux density profile is given by

$$\mathcal{F}(\theta(r)) [\text{erg s}^{-1} \text{ cm}^{-2} \text{ deg}^{-2}] = \frac{l_x(r(\theta)) d_A^2}{4\pi d_L^2} \left(\frac{\pi \text{ rad}}{180 \text{ deg}} \right)^2. \quad (\text{B2})$$

ORCID iDs

Angelo Ricarte <https://orcid.org/0000-0001-5287-0452>
 Michael Tremmel <https://orcid.org/0000-0002-4353-0306>
 Priyamvada Natarajan <https://orcid.org/0000-0002-5554-8896>

References

Alexander, T., & Natarajan, P. 2014, *Sci*, 345, 1330
 Amaro-Seoane, P., Audley, H., Babak, S., et al. 2017, arXiv:1702.00786
 Armitage, P. J., & Natarajan, P. 2002, *ApJL*, 567, L9
 Arzoumanian, Z., Baker, P. T., Blumer, H., et al. 2020, *ApJL*, 905, L34
 Baldassare, V. F., Geha, M., & Greene, J. 2020, *ApJ*, 896, 10
 Banik, U., van den Bosch, F. C., Tremmel, M., et al. 2019, *MNRAS*, 483, 1558
 Barausse, E., Dvorkin, I., Tremmel, M., Volonteri, M., & Bonetti, M. 2020, *ApJ*, 904, 16
 Barrows, R. S., Mezcua, M., & Comerford, J. M. 2019, *ApJ*, 882, 181
 Bartlett, D. J., Desmond, H., Devriendt, J., Ferreira, P. G., & Slyz, A. 2021, *MNRAS*, 500, 4639
 Begelman, M. C., Blandford, R. D., & Rees, M. J. 1980, *Natur*, 287, 307
 Bellovary, J. M., Governato, F., Quinn, T. R., et al. 2010, *ApJL*, 721, L148
 Bellovary, J. M., Hayoune, S., Chafra, K., et al. 2021, *MNRAS*, 505, 5129
 Biernacki, P., Teissier, R., & Bleuler, A. 2017, *MNRAS*, 469, 295
 Blecha, L., Loeb, A., & Narayan, R. 2013, *MNRAS*, 429, 2594
 Bondi, H. 1952, *MNRAS*, 112, 195
 Booth, C. M., & Schaye, J. 2009, *MNRAS*, 398, 53
 Bortolas, E., Capelo, P. R., Zana, T., et al. 2020, *MNRAS*, 498, 3601
 Bricman, K., & Gomboc, A. 2020, *ApJ*, 890, 73
 Butsky, I. S., Burchett, J. N., Nagai, D., et al. 2019, *MNRAS*, 490, 4292
 Cappelluti, N., Li, Y., Ricarte, A., et al. 2017, *ApJ*, 837, 19
 Chadayammuri, U., Tremmel, M., Nagai, D., Babul, A., & Quinn, T. 2021, *MNRAS*, 504, 3922
 Chandrasekhar, S. 1943, *ApJ*, 97, 255
 Chen, N., Ni, Y., Tremmel, M., et al. 2021, arXiv:2104.00021
 Comerford, J. M., Gerke, B. F., Newman, J. A., et al. 2009, *ApJ*, 698, 956
 Comerford, J. M., & Greene, J. E. 2014, *ApJ*, 789, 112
 Davis, S. W., Narayan, R., Zhu, Y., et al. 2011, *ApJ*, 734, 111
 Dubois, Y., Pichon, C., Welker, C., et al. 2014, *MNRAS*, 444, 1453
 Evans, I. N., Primini, F. A., Glotfelty, K. J., et al. 2010, *ApJS*, 189, 37
 Foord, A., Gultekin, K., Reynolds, M. T., et al. 2019, *ApJ*, 877, 17

Foord, A., Gultekin, K., Runnoe, J. C., & Koss, M. J. 2021, *ApJ*, **907**, 71

Gao, Y., Wang, Q. D., Appleton, P. N., & Lucas, R. A. 2003, *ApJL*, **596**, L171

Greene, J. E., & Ho, L. C. 2007, *ApJ*, **656**, 84

Guo, M., Inayoshi, K., Michiyama, T., & Ho, L. C. 2020, *ApJ*, **901**, 39

Hirschmann, M., Dolag, K., Saro, A., et al. 2014, *MNRAS*, **442**, 2304

Hobbs, G., Archibald, A., Arzoumanian, Z., et al. 2010, *CQGra*, **27**, 084013

Holley-Bockelmann, K., Gultekin, K., Shoemaker, D., & Yunes, N. 2008, *ApJ*, **686**, 829

Holley-Bockelmann, K., & Khan, F. M. 2015, *ApJ*, **810**, 139

Holley-Bockelmann, K., Micic, M., Sigurdsson, S., & Rubbo, L. J. 2010, *ApJ*, **713**, 1016

Hopkins, P. F., Richards, G. T., & Hernquist, L. 2007, *ApJ*, **654**, 731

Igumenshchev, I. V., & Narayan, R. 2002, *ApJ*, **566**, 137

Izquierdo-Villalba, D., Bonoli, S., Dotti, M., et al. 2020, *MNRAS*, **495**, 4681

Kaaret, P., Prestwich, A. H., Zezas, A., et al. 2001, *MNRAS*, **321**, L29

King, A. R., & Dehnen, W. 2005, *MNRAS*, **357**, 275

Knollmann, S. R., & Knebe, A. 2009, *ApJS*, **182**, 608

Kormendy, J., & Ho, L. C. 2013, *ARA&A*, **51**, 511

Koss, M., Mushotzky, R., Treister, E., et al. 2012, *ApJL*, **746**, L22

Lehmer, B. D., Basu-Zych, A. R., Mineo, S., et al. 2016, *ApJ*, **825**, 7

Libeskind, N. I., Cole, S., Frenk, C. S., & Helly, J. C. 2006, *MNRAS*, **368**, 1381

Lin, D., Strader, J., Carrasco, E. R., et al. 2018, *NatAs*, **2**, 656

Lodato, G., & Natarajan, P. 2007, *MNRAS*, **377**, L64

Ma, L., Hopkins, P. F., Ma, X., et al. 2021, arXiv:2101.02727

Matsumoto, H., Tsuru, T. G., Koyama, K., et al. 2001, *ApJL*, **547**, L25

Mezcua, M., Civano, F., Marchesi, S., et al. 2018, *MNRAS*, **478**, 2576

Mezcua, M., & Domínguez Sánchez, H. 2020, *ApJL*, **898**, L30

Miller, J. M., Fabbiano, G., Miller, M. C., & Fabian, A. C. 2003, *ApJL*, **585**, L37

Natarajan, P. 2021, *MNRAS*, **501**, 1413

Neumayer, N., Seth, A., & Böker, T. 2020, *A&ARv*, **28**, 4

Pellegrini, S. 2005, *ApJ*, **624**, 155

Perna, R., Narayan, R., Rybicki, G., Stella, L., & Treves, A. 2003, *ApJ*, **594**, 936

Pesce, D. W., Seth, A. C., Greene, J. E., et al. 2021, *ApJ*, **909**, 141

Pfister, H., Volonteri, M., Dubois, Y., Dotti, M., & Colpi, M. 2019, *MNRAS*, **486**, 101

Pontzen, A., Roškar, R., Stinson, G., & Woods, R. 2013, pynbody: N-Body/SPH Analysis for Python, Version 1.0.9, Astrophysics Source Code Library, ascl:1305.002

Pontzen, A., & Tremmel, M. 2018, *ApJS*, **237**, 23

Power, C., Navarro, J. F., Jenkins, A., et al. 2003, *MNRAS*, **338**, 14

Rees, M. J. 1988, *Natur*, **333**, 523

Reines, A. E., Condon, J. J., Darling, J., & Greene, J. E. 2020, *ApJ*, **888**, 36

Reines, A. E., & Volonteri, M. 2015, *ApJ*, **813**, 82

Ressler, S. M., Quataert, E., White, C. J., & Blaes, O. 2021, *MNRAS*, **504**, 6076

Ricarte, A., Tremmel, M., Natarajan, P., & Quinn, T. 2019, *MNRAS*, **489**, 802

Ricarte, A., Tremmel, M., Natarajan, P., Zimmer, C., & Quinn, T. 2021, *MNRAS*, **503**, 6098

Sanchez, N. N., Werk, J. K., Tremmel, M., et al. 2019, *ApJ*, **882**, 8

Schramm, M., & Silverman, J. D. 2013, *ApJ*, **767**, 13

Steinborn, L. K., Dolag, K., Comerford, J. M., et al. 2016, *MNRAS*, **458**, 1013

Stemo, A., Comerford, J. M., Barrows, R. S., et al. 2020, arXiv:2011.10051

Stone, N. C., & Metzger, B. D. 2016, *MNRAS*, **455**, 859

Stone, N. C., Vasiliev, E., Kesden, M., et al. 2020, *SSRv*, **216**, 35

Strubbe, L. E., & Quataert, E. 2009, *MNRAS*, **400**, 2070

Tamfal, T., Capelo, P. R., Kazantzidis, S., et al. 2018, *ApJL*, **864**, L19

Tremmel, M., Governato, F., Volonteri, M., Pontzen, A., & Quinn, T. R. 2018a, *ApJL*, **857**, L22

Tremmel, M., Governato, F., Volonteri, M., & Quinn, T. R. 2015, *MNRAS*, **451**, 1868

Tremmel, M., Governato, F., Volonteri, M., Quinn, T. R., & Pontzen, A. 2018b, *MNRAS*, **475**, 4967

Tremmel, M., Karcher, M., Governato, F., et al. 2017, *MNRAS*, **470**, 1121

Tremmel, M., Quinn, T. R., Ricarte, A., et al. 2019, *MNRAS*, **483**, 3336

van den Bosch, F. C., & Ogiya, G. 2018, *MNRAS*, **475**, 4066

van Velzen, S., Farrar, G. R., Gezari, S., et al. 2011, *ApJ*, **741**, 73

Voggel, K. T., Seth, A. C., Baumgardt, H., et al. 2019, *ApJ*, **871**, 159

Volonteri, M. 2007, *ApJL*, **663**, L5

Volonteri, M., Dubois, Y., Pichon, C., & Devriendt, J. 2016, *MNRAS*, **460**, 2979

Volonteri, M., Haardt, F., & Madau, P. 2003, *ApJ*, **582**, 559

Volonteri, M., & Perna, R. 2005, *MNRAS*, **358**, 913

Volonteri, M., Pfister, H., Beckmann, R. S., et al. 2020, *MNRAS*, **498**, 2219